Nonreciprocal quantum information processing with superconducting diodes in circuit quantum electrodynamics

Nicolas Dirnegger,¹ Prineha Narang,^{1,2,*} and Arpit Arora^{1,2,†}

¹Department of Electrical and Computer Engineering, UCLA, Los Angeles, CA, USA

²Division of Physical Sciences, College of Letters and Science,
University of California, Los Angeles (UCLA), Los Angeles, CA, USA

Introducing new components and functionalities into quantum devices is critical in advancing state-of-the-art hardware. Here, we propose superconducting diodes (SDs) as a coherent nonreciprocal element in circuit quantum electrodynamics (cQED) architectures. In particular, we use an asymmetric SQUID as an SD controlled with a flux bias. We spectroscopically characterize SD and show that flux bias acts cooperatively with the nonlinear diode response to induce direction-dependent resonance shifts in the transmission spectrum. We use the SD as an elementary component to realize coherent nonreciprocal qubit-qubit coupling. With a minimal two qubit system, we demonstrate a nonreciprocal half-iSWAP gate with tunable Bell-state generation, thereby showcasing the potential of intrinsic nonreciprocity as a tool in coherent control in quantum technologies. Our work enables high-fidelity signal routing and entanglement generation in all-to-all connected microwave quantum networks, where nonreciprocity is embedded at the device level.

Introduction

Nonreciprocal transfer of quantum states and correlations is crucial for scalable devices and networks [1–4]. In superconducting circuits, nonreciprocity is typically realized using commercially available ferrite-based components, which introduce loss and are incompatible with on-chip integration [5]. Alternate schemes based on superconductors have been proposed based on magnon coupling [6, 7], geometric designs [8–10], and reservoir engineering [11–13], to name a few. Although effective, these

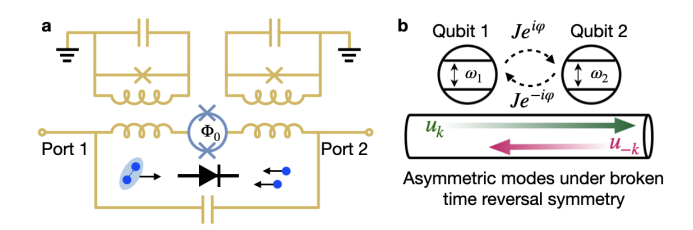


FIG. 1: Superconducting diode (SD) and nonreciprocal qubit-qubit coupling: (a) Circuit of two qubits inductively coupled to a SD. Here, the SD is formed by an asymmetric SQUID (shown in blue) which is biased by external flux, Φ_0 . The supercurrent is allowed along the direction of forward bias (shown as bound Cooper pairs), and is blocked along the direction of reverse bias (shown as broken Cooper pairs). (b) Schematic of nonreciprocal coupling due to SD. The broken time reversal (\mathcal{T})-symmetry necessary to induce a diode response generically makes the coupling between qubits to be complex, $J_{12} = Je^{i\phi_{12}}$ with non-local phase $\phi_{12} = \varphi$ is determined by nonreciprocal response by asymmetric mode propagation in SD.

components have a large footprint, and active modulation adds complexity and noise. As a result, the search continues for coherent, hardware-level nonreciprocal element that can be embedded directly into superconducting circuits, enabling the design of robust and scalable quantum processors.

The recently discovered superconducting diode (SD) effect [14–19] opens a new paradigm for realizing intrinsic nonreciprocal elements [20-22]. SDs are characterized by direction-dependent critical currents, and have been realized in bulk superconductors, Josephson junctions (JJs), and superconducting quantum interference devices (SQUIDs) [14]. Unlike conventional routes of nonreciprocity that rely on engineering losses [23, 24], the superconducting diode effect arises from a fundamental asymmetry in the system response, enabled by breaking inversion (\mathcal{I}) and time-reversal symmetry (\mathcal{T}) [15, 25– 27]. Importantly, nonreciprocity is property of the superconducting ground state[18, 28], fully captured by the free energy and the evolution of the superconducting order parameter. This functionality can be harnessed through numerous means including magnetic flux [29], spin-orbit coupling [30], spontaneously symmetry broken states [31], SQUIDs [32], conformally mapped materials [33] or even with chiral microwaves [34, 35].

In this work, we utilize the principles of SD-based non-reciprocity: passive nonreciprocity demonstrated by the coherent device response controlled by a single control line. In particular, we consider the asymmetric SQUID as an SD with a flux-switching bias which cooperates with nonlinear inductance to enable the nonreciprocal response, as shown in Fig. 1. We calculate the transmission spectrum of the SD in a circuit quantum electrodynamics (cQED) setup, featuring an asymmetric mode structure with direction-dependent resonance shifts. We then obtain coherent nonreciprocal qubit-qubit interactions determined by complex coupling mediated by the SD. We analyze the corresponding qubit population dynamics, and implement a nonreciprocal entangling gate [36] us-

^{*}Electronic address: prineha@ucla.edu †Electronic address: arpit22@ucla.edu

ing this architecture, demonstrating directional control over Bell-state formation. Finally, we show tomographic representation of Bell states, and highlight direct experimental signatures. These results establish the SD as a resource of nonreciprocity embedded at the device level and a scalable building block for directional quantum control.

Superconducting diode and its spectroscopic characterization

The SD effect is a magnetoelectric nonlinear response in superconductors and superconducting devices. Microscopically, the diode behavior emerges from a shift in Cooper pair center of mass, fundamentally realized by simultaneous breaking of \mathcal{T} and \mathcal{I} symmetries which in JJ and SQUID based devices can be tuned with Cooper pair transmission and phase accumulation across each junction [14, 37]. The SD is characterized diode efficiency [15, 19]

$$\eta = \left| \frac{I_c^+ - I_c^-}{I_c^+ + I_c^-} \right| \tag{1}$$

where I^{\pm} is the current in forward/backward direction, and I_c^{\pm} is the corresponding critical current. Recent experiments have demonstrated SD behavior in a variety of platforms, including noncentrosymmetric thin films such as Nb₃Br₈ [38], proximitized semiconductors with spinorbit coupling (e.g., InAs/Al Josephson junctions) [39–41], and asymmetric SQUID architectures [42, 43]. Additionally, magnetic-field-free diodes have been created from graphene-based devices [44] and high temperature effect has been reported for anomalous cuprate junctions [45].

Here, we consider an SD formed by an asymmetric SQUID, where the diode response is controlled by external bias flux (Φ_b , see Fig. 1) [46]. The asymmetric SQUID is characterized by the potential $U(\Phi) = U_1(\Phi) +$ $U_2(\Phi - \Phi_b)$, where $U_{1,2}(\Phi) = -\Delta[1 - \tau_{1,2}\sin^2(\Phi/2)]^{1/2}$ is the Josephson potential of JJs in the SQUID, $\tau_{1,2}$ is the respective junction transmission, and Δ is the superconducting gap. The diode respose arises from \mathcal{T} , \mathcal{I} -broken quantum interference between high and low transmission Andreev bound states in the SQUID: \mathcal{T} is broken by $\Phi_b \neq n\pi \ (n \in \text{integer}) \text{ and } \mathcal{I} \text{ is broken by } \tau_1 \neq \tau_2.$ In other words, current phase relation becomes nonreciprocal due to superposition of fundamental harmonic with higher order harmonics. We summarize the fundamentals of diode response in the SQUID in Supplementary Information (SI) section S1.

We define the notion of directionality and bias of the SD: sign of flux, Φ_b , sets the bias of diode and applied current, $I_a = I^{\pm}$, sets the signal directionality. In other words, $\Phi_b = \pm |\Phi_b|$ sets the diode in forward (reverse) bias allowing $I_a = I_{\pm}$ to pass and blocking $I_a = I_{\mp}$. For cQED modalities this translates to nonreciprocity in kinetic inductance, $L_{\pm} = L_0 \left[1 + (I_a/I_c^{\pm})^2 \right]$ where L_0 is the characteristic circuit inductance. This can be directly

seen in spectroscopic signatures when the SD is shunted to a capacitor, C with transmission spectrum peak at $\omega_r^{\pm} = 1/\sqrt{L^{\pm}C}$. This enables a single flux-line tunable nonreciprocal resonator.

The corresponding frequency shift due to nonreciprocal device response can be obtained using the lumped element measurement where the measured frequency is $\omega_{\pm}=\omega_r\sqrt{L_0/L_{\pm}}.$ We have defined $\omega_r=1/\sqrt{L_0C}$ as the characteristic frequency of the circuit. The shift in resonance is $\delta\omega_{\pm}/\omega_r\approx-0.5(I_a/I_{\pm})^2.$ For diode response, we have $I_+\neq I_-$ leading to $L_+\neq L_-.$ For $\eta\approx20\%,$ we have $I_c^+/I_c^-=3/2$ which corresponds to $L_K^--L_K^+=5L_0I_a^2/[9(I_c^-)^2].$ Then, we estimate $\delta\omega=\delta\omega_--\delta\omega_+$ using standard cQED experimental inputs $\omega_0=5$ GHz, $I_a=30$ nA and $I_-=150$ nA which corresponds to $\delta\omega\approx55$ MHz.

The nonreciprocal behavior can be tracked via transmission spectrum. We follow standard recipe of inputoutput theory (also see SI section S2), according to which $S_{ji}(\omega) = Z_0/(Z_0 + Z_{ji}(\omega))$ where $S_{ji}(\omega)$ is the transmission, $Z_{ji}(\omega)$ is the impedance response of the circuit and Z_0 is the matched impedance between the two ports. For resistance R in the circuit $Z_{ji}(\omega) = R + i[\omega L_{ji} - (\omega C)^{-1}]$, and for SD $L_{ji} \neq L_{ij}$. Consequently, we obtain forward $S_+(\omega) = S_{21}(\omega)$ and backward transmission $S_-(\omega) = S_{12}(\omega)$ as

$$S_{\pm}(\omega) = \frac{\mathcal{A}_{\pm}}{(\omega - \omega_{\pm})^2 + \kappa_{\pm}^2} \tag{2}$$

where $\mathcal{A}_{\pm}=(Z_0/2L_{\pm})^2$ and $\kappa^{\pm}=Z_0+R/2L_{\pm}$. Crucially, with $S_+(\omega)\neq S_-(\omega)$ Eq. (2) serves as the central relation to the benchmark an SD. In Fig. 2a,b, we show the transmission spectrum calculated using Heisenberg-Langevin equations at mean-field level for $\delta\omega=0$ and 50 MHz, respectively. We account for Kerr nonlinearity, drive and interaction with environment to show that the SD induced nonreciprocity is robust. In Fig. 2c, we show the nonreciprocity ratio

$$\mathcal{R}(\omega) = \frac{|S_{+}(\omega)| - |S_{-}(\omega)|}{|S_{+}(\omega)| + |S_{-}(\omega)|} \tag{3}$$

providing a measure of forward-to-backward asymmetry at each frequency. We identify $\mathcal{R}(\omega)$ magnitudes are largest at $\omega = \omega_r^{\pm}$. Interestingly, significant $\mathcal{R}(\omega) \neq 0$ maintains even away from $\omega = \omega_{\pm}$ implying that non-reciprocities can be efficiently used even for off-resonant device operations.

Next, as a proof of concept, we elucidate the microscopic origin of SD nonreciprocity using the canonical Hamiltonian for SD shunted to capacitor: $H_r = 4E_cN + U(\Phi)$ where E_c is the charging energy and $U(\Phi)$ is the Josephson energy potential. We Taylor expand $U(\Phi) = \sum_n \frac{c_n}{n!} (\Phi - \Phi_{\min})^n$ around minima Φ_{\min} obtained self-consistently by solving $c_1 = \partial_{\Phi} U(\Phi) = 0$ [22]. The diode nonreciprocity emerges as a third order nonlinearity, $c_3(\Phi_b)\Phi^3/6$ with $c_3 = \partial_{\Phi}^3 U(\Phi)|_{\Phi_{\min}}$. Note that $c_3(\Phi_b) \neq 0$ explicitly breaks \mathcal{T} as $U(-\Phi) \neq U(\Phi)$, and it

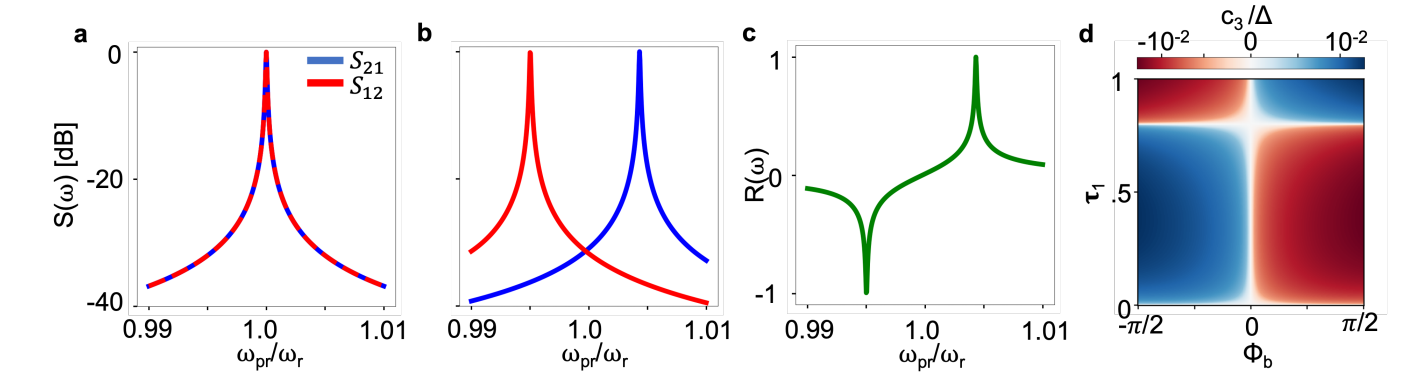


FIG. 2: Spectroscopic characterization of superconducting diode on a two-port network: (a) Transmission spectrum at fixed off-resonant pump frequency $\omega_p/\omega_r=0.99$, normalized by resonator frequency $\omega_r=5$ GHz, shows scattering matrix $S(\omega)$ with respect to probe frequency ω_{pr}/ω_r for $\delta\omega=0$. (b) Transmission spectrum with $\delta\omega=50$ MHz showing clear asymmetric shift between S_{21} and S_{12} . (c) Nonreciprocity ratio, $R(\omega)$, for same parameters as in panel (b). For all simulations the following parameter were used $\omega_p/\omega_r=0.99$, Kerr nonlinearity $\Lambda/\omega_r=10^{-7}$, two photon loss $\kappa/\omega_r=10^{-4}$. (d) Third-order Josephson nonlinearity, c_3/Δ with , for the asymmetric SQUID versus flux Φ_b , and transmission, τ_1 ($\tau_2=0.8$).

is odd with respect to Φ_b vanishing identically at $\Phi_b = 0$, see Fig. 2d. This contribution has been known as a source of three-wave mixing, seen also in Josephson ring modulators [47], and recently discussed in Ref. [48] in context of minimizing Kerr-nonlinearity in SDs, akin to SNAIL parametric amplifiers [22, 49]. The combination of $\Phi_b, c_3(\Phi_b) \neq 0$ leads to bias and direction controlled resonance shifts which can be obtained by transforming to bosonic operators. We define

$$\Phi(x) = \sum_{k} \Phi_{\text{zpf}} \left[\psi_k(x) a_k + \psi_k^*(x) a_k^{\dagger} \right]$$
 (4)

where a_k is the bosonic operator, and $\psi_k(x) = u_k e^{ikx}$ is the mode function between the ports; $\Phi_{\rm zpf}$ is the flux at zero point fluctuation. Within mean-field treatment we write $a_k = \alpha_k + d_k$ where $\langle a_k \rangle = \Phi_b \alpha_k$ is the mean-field expectation value satisfying $\langle \Phi \rangle = \Phi_b$ and $\langle d_k \rangle = 0$. The third order nonlinearity in Josephson potential at leading order in Φ_b gives $c_3(\Phi_b)\Phi_b\sum_k d_k^{\dagger}d_k$ where the bilinear form of the bosonic operators beyond three-wave mixing together with $u_{-k}^* \neq u_k$ under broken- $\mathcal T$ results in direction dependent resonance frequency shift, $\delta \omega = \omega_k - \omega_{-k}$ such that

$$\delta\omega = \operatorname{sgn}(\Phi_b)|c_3(\Phi_b)\Phi_b\mathcal{F}_k(\Phi_b)| \tag{5}$$

where $\mathcal{F}_k(\Phi_b)$ captures the geometry dependent factor odd in Φ_b due to mode asymmetry, $u_k \neq u_{-k}^*$, see SI section S3 for details. Therefore, we have a resonator with flux-controlled resonance shifts when the system responds with $c_3(\Phi_b) \neq 0$ under broken \mathcal{T} and \mathcal{I} .

Nonreciprocal qubit-qubit coupling by SD

Having established characterization of the nonreciprocal SD through Fig. 2 and Eq. (2), we use it to induce nonreciprocal coupling between qubits. We consider a 2-qubit (Q_1, Q_2) system for brevity but our approach is valid for n-qubits connected through a single resonator [50]. The effective Hamiltonian for the 2-qubit system in leading order in qubit operators can be generically expressed as

$$\mathcal{H} = \sum_{i} \frac{\omega_{i}}{2} \sigma_{z}^{(i)} + \sum_{i \neq j} J_{ij} (\sigma_{-}^{(i)} \sigma_{+}^{(j)} + \text{h.c.})$$
 (6)

where $\sigma_{\pm}^{(i)} = \sigma_x^{(i)} \pm \sigma_y^{(i)}$ and $\sigma_{x,y,z}^{(i)}$ is Pauli operator for qubit at port $i \in \{1,2\}$. Here, ω_i is the excitation energy of qubit i and J_{ij} is the interaction between nearest neighbor qubits i and j. Importantly, J_{ij} captures the nonreciprocity carried by the SD resonator, and can be expressed with a complex phase

$$J_{ij} = |J|e^{i\phi_{ij}}. (7)$$

where J is the strength of the coupling and ϕ_{ij} is a non-local phase governing the nonreciprocal interactions between qubits located at different ports of the resonator.

Phenomenologically, Eq. (7) captures fundamental nonreciprocity in any system breaking \mathcal{T} symmetry [20, 23, 51, 52]. To track its microscopic origin within the diode response of SD, we calculate the qubit-qubit coupling

$$J_{ij} = g^2 \sum_{k} \mathcal{G}_{ij,k}(\omega) \tag{8}$$

by evaluating the causal Green's function between the ports, $\mathcal{G}_{ij,k} = \psi_k(x_i)\chi_k(\omega)\psi_k(x_j)^*$ with $\chi_k(\omega) = [(\omega - \omega_k) + i\kappa]^{-1}$; κ is two photon decay. Without loss of generality we have assumed qubits couple to resonator identically with coupling strength g, and mode amplitudes are defined as in Eq. (4). We decompose the Green's function into forward and backward traversing modes such

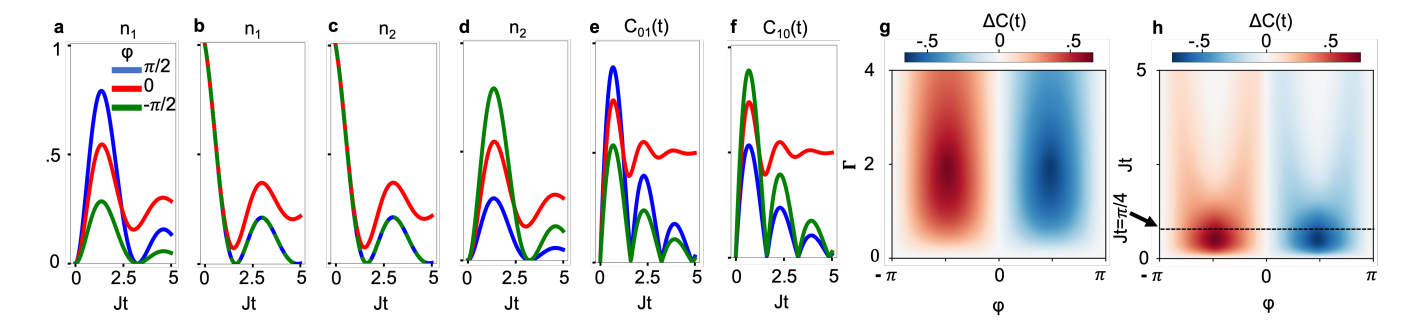


FIG. 3: Coherent control of population dynamics via effective qubit-qubit coupling through SD and dynamic evolution of concurrence in two qubit system. (a-d) The population dynamics of qubits $n_1(t), n_2(t)$ at $\varphi \in [-\pi/2, 0, \pi/2]$ (green, red and blue lines). Panels a,b show $n_1(t), n_2(t)$, respectively with $n_1(t=0), n_2(t=0)=1$, and the system initialization is reversed in panels c,d. (e,f) Concurrence C_{01} and C_{10} plotted against Jt for different $\varphi \in [-\pi/2, 0, \pi/2]$. For $\varphi = 0$ (red) the concurrence C_{01} and C_{10} are identical. For $\varphi = \pm \pi/2$ (blue for C_{01} and green for C_{10}), we observe that the concurrence grows close to 1.0 signaling maximal entanglement at time scale of half-iSWAP facilitated by SD nonreciprocity. (g) Heatmap for entanglement transfer contrast, $\Delta C(t)$ at $t = \pi/4J$ as a function of φ and Γ . $\Delta C(t = \pi/4J)$ is maximum at $\Gamma/J = 2$ and $\varphi = \pm \pi/2$, and significant nonreciprocity sustains throughout the phase space. (h) $\Delta C(t)$ in variation with Jt and φ showing maximum entanglement contrast at $\varphi = \pm \pi/2$ at the scale of time of half-iSWAP. All plots were made with following parameters $\gamma_1 = 0$, J = 1, $\Gamma = 0.5$, unless mentioned otherwise.

that $\mathcal{G}_{ij,k} = \mathcal{G}_{ij,+k} + \mathcal{G}_{ij,-k}$ and restrict the summation in Eq. (8) to k > 0. This allows us to extract the reciprocal and nonreciprocal counterparts of the coupling such that $J_{ij} = J_{ij}^{\rm r} + i J_{ij}^{\rm nr}$ reproducing Eq. (7) with the non-local phase

$$\phi_{ij} = \tan^{-1} \left(\frac{J_{ij}^{\text{nr}}}{J_{ij}^{\text{r}}} \right) \tag{9}$$

characterized by the non-reciprocal response of the system

$$J_{ij}^{\rm nr} = g^2 \sum_{k>0} |\chi_k(\omega)|^2 \sin[k(x_j - x_i)] \delta\omega.$$
 (10)

Importantly, we have obtained SD determined nonreciprocal qubit-qubit coupling which is a consequence of fundamental device response and controlled by Φ_0 and direction of signal, see Eq. (5) and Eq. (10) – $J_{ij}^{\rm nr}$ flips sign with Φ_b and $(x_i \leftrightarrow x_j)$. Strikingly, Eq. (7,9) match up with general nonreciprocal coupling obtained in Ref. [20] for a general \mathcal{T} -broken quantum model.

In what follows, we use $\phi_{ij} = \varphi$ as a parameter to demonstrate nonreciprocal qubit dynamics for Eq. (6). Before proceeding to demonstrate the nonreciprocity, we emphasize that $\phi_{ij} \neq 0$ is determined by the behavior of SD, and allows control of nonreciprocity of the system by device response, unlike existing paradigms which rely on dissipation controlled non-Hermitian dynamics of the system. However, given the passive nature of nonreciprocity, the presence of drive or dissipation is necessary to translate SD characteristics to system dynamics. Nevertheless, as we show below the control handle is completely determined by control over SD.

We model the dynamics of our minimal system consisting of SD resonator coupled to two gubits as an open

quantum system and following standard recipe of Lindblad master equation track qubit population through time evolution of σ_z

$$\dot{\sigma}_{z}^{(i)} = -\gamma_{1,i} \left(\sigma_{z}^{(i)} + 1 \right) - 2i \sum_{j \neq i} J_{ij} \left(\sigma_{+}^{(i)} \sigma_{-}^{(j)} - \sigma_{+}^{(j)} \sigma_{-}^{(i)} \right) - \sum_{j \neq i} \Gamma \left(\sigma_{+}^{(i)} \sigma_{-}^{(j)} + \sigma_{+}^{(j)} \sigma_{-}^{(i)} \right), \tag{11}$$

where we have accounted for qubit relaxation $(\gamma_{1,i})$ and collective cross-qubit decay (Γ) . The qubit population is obtained as $n_i(t) = \langle \sigma_z^{(i)}(t) \rangle$. The qubit initialization is described in terms of initial condition of Eq. (11), $n_i(t=0)$.

In Fig. 3a,b, we show $n_{1,2}(t)$ with $n_{1,2}(t=0)=0,1$, and in Fig. 3c,d we show $n_{1,2}(t)$ with flipped system initialization, $n_{1,2}(t=0)=1,0$. When $\varphi=0$ (red curves), the population dynamics are reciprocal: regardless of whether qubit-1 or qubit-2 is initially excited, the subsequent time evolution is identical, reflecting symmetric coupling between the two modes. In contrast, for $\varphi = \pm \pi/2$ (blue and green curves), the dynamics become nonreciprocal. Depending on the sign of φ , excitation transfer is either enhanced or suppressed in one direction as compared to the other, leading to a pronounced directional asymmetry. This phase-controlled nonreciprocal population transfer effectively mimics isolation: the system favors energy flow in one direction while inhibiting it in the reverse. This demonstraates SD as an intrinsic and easily controlled fab-level integrated nonreciprocal component. At long times, the exponential decay of all curves reflects intrinsic dissipation, which sets the overall relaxation timescale.

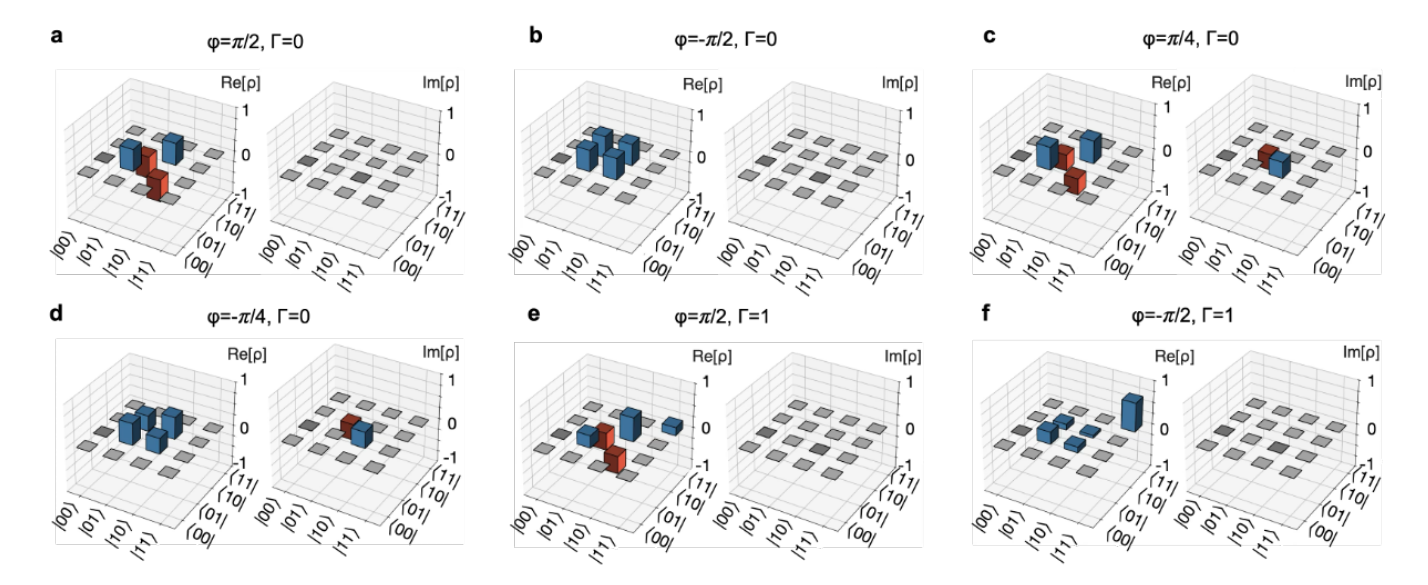


FIG. 4: Bell state tomographic representation of density matrices of the qubit pairs via linear reconstruction after half-iSWAP $(t=\pi/4J)$ applied to qubits. The system is initialized to $\Psi(t=0)=|01\rangle$ for all panels. (a-d) $\mathbf{Re}[\rho]$ and $\mathbf{Im}[\rho]$ without account of decays, γ_1 , $\Gamma=0$ for $\varphi\in[\pi/2,-\pi/2,\pi/4,-\pi/4]$ reproducing Bell state derived in Eq. (12). Blue colors represent positive values while red represent negative values. Tunable Bell-states are formed with non-trivial phase captured in $\mathbf{Im}[\rho]\neq 0$. (e-f) Tomographic reconstruction of density matrix with collective cross decay, $\Gamma/J=1$ at $\varphi=\pm\pi/2$. The Bell state generation is nonreciprocal determined by cooperative action of diode nonreciprocity and decay. For $\varphi=\pi/2$, $|\Psi_-\rangle$ is generated with nearly 80% fideltiy and for $\varphi=-\pi/2$ no Bell state is formed as fidelity remains below 50% (nearly 30%). This demonstrates the diodes ability to generate and distribute entanglement directionally between the qubit systems.

Directional half-iSWAP gate

To leverage the nonreciprocal dynamics in context of quantum information processing, we next demonstrate a directional half-iSWAP gate. We project the Hamiltonian in Eq. (6) onto the one-excitation subspace $\{|10\rangle, |01\rangle\}$. Starting with $|\Psi(t=0)\rangle = |01\rangle$, the corresponding entangled state at the time of half-iSWAP, $t=\pi/4J$, is then obtained as (see SI section 5)

$$|\Psi(t=\pi/4J)\rangle = \frac{1}{\sqrt{2}} \left(|10\rangle + ie^{i\varphi}|01\rangle \right),$$
 (12)

and the standard Bell states are obtained at $\varphi=\pm\pi/2$. Such tunability of symmetric and asymmetric combination of wavefunctions is reminiscent of tunable couplers [53, 54]. However, in contrast to tunable couplers the entanglement generation, as we show below, is nonreciprocal. Additionally, the diode enables versatile entanglement generation controlled by the φ leading to new channels in two-gate entangling operations. Such control over entangled states in single operation is seldom in superconducting circuits, and limited to interferometry entangled photonic states [55] or optically controlled spin-qubits [56].

To highlight the phase-controlled directionality of entanglement transfer, we evaluate the concurrence C(t) following Ref. [57], which quantifies bipartite entanglement on a scale from 0 (separable) to 1 (maximally entangled). Figures 3e.f show the time evolution of

 $C_{01}(t)$ and $C_{10}(t)$ corresponding to system initialization at $|\Psi(t=0)\rangle = |01\rangle$ and $|\Psi(t=0)\rangle = |10\rangle$, respectively. For $\varphi = 0$, the concurrence dynamics are symmetric and yield identical entanglement generation for both initial conditions. In contrast, for $\varphi \neq 0$, the dynamics become strongly asymmetric: for $\varphi = +\pi/2$ the entanglement generated when qubit 1 is initially excited is significantly enhanced with maximal entanglement achieved at scale of half-iSWAP execution time, $t = \pi/4J$. For $\varphi = -\pi/2$ the situation is reversed, with maximal entanglement occurring when qubit 2 is initially excited. This selective enhancement and suppression of entanglement transfer reflects the underlying nonreciprocal interaction engineered through the diode coupler.

In Figs. 3g, we show the entanglement transfer contrast $\Delta C(t) = C_{01}(t) - C_{10}(t)$ as a function of φ and Γ at $t = \pi/4J$. Previous studies on two-port nonreciprocal qubit coupling relied on dissipation engineering to find sweet-spot in parameter space at $2J = \Gamma$ [23, 58]. Strikingly, in contrast we find that though presence of dissipation is necessary given the passive of nature of SD nonreciprocity but high degree of isolation is achievable even away from $2J = \Gamma$. This can be seen as wide spread blue (for $\varphi > 0$) and red (for $\varphi < 0$) regions where $|01\rangle$ initialized |10\rangle initialized states dominate, respectively. This difference marks an important distinction of SD based nonreciprocity from schemes proposed in previous art [23, 58]. Moreover, the complete isolation regime is now tunable by a single flux control affecting the coherent response. Finally, in Fig. 3h, we show $\Delta C(t)$ in variation with φ and t at $\Gamma=J$, and note maximal isolation around $\varphi=\pm\pi/2$ and $t=\pi/4J$. The transient character of peaks indicates dominant coherent interactions driving nonreciprocal entanglement dynamics at scale of half-iSWAP time.

To verify that the nonreciprocal transient quantum correlation really corresponds to a Bell-type superposition shown in Eq. 12, we perform full two-qubit state tomography at the half-iSWAP time $t=\pi/4J$. We stimulate the standard 16-basis measurement protocol [59–73] (combinations of $\{I,X,Y,Z\}$ on each qubit) using linear reconstruction. While our starting point is the numerically evaluated Bell state in presence of qubit relaxation (γ_1) and collective cross-decay (Γ) , the tomographic representation provides benchmark signals to probe SD mediated nonreciprocal entanglement generation.

We begin by setting $\gamma_1 = \Gamma = 0$ to understand the effect of $\varphi \neq 0$ in Bell state in Eq. (12) in terms of tunable entanglement generation. This directly reflects in real $(\mathbf{Re}[\rho])$ and imaginary $(\mathbf{Im}[\rho])$ parts of off-diagonal elements of density matrix. In Fig. 4a,b, we show the density matrix corresponding to $|\Psi(t=\pi/4J,\varphi=\pm\pi/2)\rangle$ with $|\Psi(t=0)\rangle = |10\rangle$ generating the usual Bell states $|\Psi_{\mp}\rangle = \frac{1}{2}(|10\rangle \mp |01\rangle)$, and $\mathbf{Im}[\rho] = 0$ throughout. The Bell state are flipped when $|\Psi(t=0)\rangle = |01\rangle$, and when $\varphi = 0$, same Bell pair $|\Psi(t=\pi/4J,\varphi=0) = \frac{1}{2}(|10\rangle + i|01\rangle)$ is generated irrespective of system initialization. Similarly, other nontrvial $\varphi \neq 0$ can be tracked with Bell state reconstruction. For instance, $\varphi = \pm \pi/4$ is reflected as complex values of off-diagonal elements of reconstructed denisty matrix, see Fig. 4c,d.

Next, we introduce the cross-qubit decay, $\Gamma \neq 0$ which facilitates passive SD nonrecirpcoty in isolation of generated Bell pairs. In Fig. 4e,f we show reconstructed density matrix for $\varphi = \pm \pi/2$, and we clearly note nonreciprocal entanglement generation. For simulated reconstructed density matrix, we find formation of $|\Psi_{-}\rangle$ for $\varphi = \pi/2$ with nearly 80% fidelity for $\Gamma = J$. On the contrary, for $\varphi = \pi/2$, we find that fidelity remains below 50% (nearly 30%) for $\Gamma = J$ and targetted entangled state is not generated. Taken together with the concurrence dynamics [Figs. 3e-h], these results establish the role of SD as a tunable, nonreciprocal entangling coupler, enabling selective and phase-programmable entanglement routing between remote qubits. Beyond this specific device, the same operating principle and our analysis naturally extends to high-quality, long-distance qubit interconnects [4], providing a powerful resource for modular and directional quantum network architectures.

Conclusion

In conclusion, we have presented the SD as a coherent and passive nonreciprocal element featuring a single control handle capable of directional quantum state transfer determined by its intrinsic device response. This functionality was most transparently demonstrated with

a minimal two-qubit architecture, and can be naturally extended to multi-qubit systems and distributed interconnects [73, 74]. We considered an asymmetric SQUID realization of the SD [75, 76], which can be readily integrated with state-of-the-art circuit-QED hardware [13]. The spectroscopic characterization and Bell-state reconstruction benchmarks developed here provide practical routes for implementing these functionalities in near-term experiments.

Looking forward, our demonstration of intrinsic superconducting nonreciprocity opens a clear path to onchip signal routing and isolation without bulky circulators [70, 77, 78]. By embedding SD resonators directly into cQED chips, one can dramatically reduce cryogenic wiring and footprint. The SD's single handle "on/off" knob also promises hardware-level multiplexing and demultiplexing, cutting resource overhead by orders of magnitude. Tunable nonreciprocal phases afford a versatile tool to realize directional two- and multi-qubit gates (e.g. cascaded iSWAP chains) [8, 79] and potentially for engineering chiral multi-body interactions [24].

Exploring these gates within small repetition or surface-code modules may yield improved fault-tolerance thresholds through reduced back-action [80]. Larger networks of SD couplers naturally implement synthetic gauge fields in a coherent, lossless platform, enabling directional quantum memories, quantum Hall analogues, and protected edge-mode state transfer [51, 81, 82].

Moving beyond proof-of-principle, key next steps include device optimization, detailed coherence studies, and full-chip simulations of SD-interconnected qubit lattices [83]. Ultimately, embedding nonreciprocal superconducting elements at the device level could transform how we build modular processors.

Acknowledgments

We acknowledge helpful discussions with William Oliver, Joel Wang, Aziza Almanakly, David Pahl and Murat Can Sarihan for providing device level insights and useful comments on the manuscript. We also thank Lukas Baker, Othmane Benhayoune-Khadraoui, and William Munizzi for useful discussions. This work was supported by the Defense Advanced Research Projects Agency (DARPA), Quantum Science Center (a National Quantum Information Science Center of the U.S. Department of Energy), Gordon and Betty Moore Foundation (Grant Numbers GBMF8048 and GBMF12976), and the John Simon Guggenheim Memorial Foundation (Guggenheim Fellowship).

References

 S. Wehner, D. Elkouss, and R. Hanson, Science 362, 9288 (2018).

- [2] B. Kannan, A. Almanakly, Y. Sung, A. Di Paolo, D. A. Rower, J. Braumüller, A. Melville, B. M. Niedzielski, A. Karamlou, K. Serniak, A. Vepsäläinen, M. E. Schwartz, J. L. Yoder, R. Winik, J. I.-J. Wang, T. P. Orlando, S. Gustavsson, J. A. Grover, and W. D. Oliver, Nature Physics 19, 394 (2023).
- [3] S. Barzanjeh, A. Xuereb, A. Alù, S. A. Mann, N. Nefedkin, V. Peano, and P. Rabl, arXiv preprint arXiv:2508.03945 (2025).
- [4] A. Almanakly, B. Yankelevich, M. Hays, B. Kannan, R. Assouly, A. Greene, M. Gingras, B. M. Niedzielski, H. Stickler, M. E. Schwartz, et al., Nature Physics, 1 (2025).
- [5] A. Kord, D. L. Sounas, and A. Alu, Proceedings of the IEEE 108, 1728 (2020).
- [6] Y.-Y. Wang, S. van Geldern, T. Connolly, Y.-X. Wang, A. Shilcusky, A. McDonald, A. A. Clerk, and C. Wang, Physical Review Applied 16, 064066 (2021).
- [7] Y.-T. Chen, L. Du, L. Guo, Z. Wang, Y. Zhang, Y. Li, and J.-H. Wu, Communications Physics 5, 215 (2022).
- [8] K. Sliwa, M. Hatridge, A. Narla, S. Shankar, L. Frunzio, R. Schoelkopf, and M. Devoret, Physical Review X 5, 041020 (2015).
- [9] C. Müller, S. Guan, N. Vogt, J. H. Cole, and T. M. Stace, Physical review letters 120, 213602 (2018).
- [10] R. Navarathna, D. T. Le, A. R. Hamann, H. D. Nguyen, T. M. Stace, and A. Fedorov, Physical review letters 130, 037001 (2023).
- [11] P. Krantz, M. Kjaergaard, F. Yan, T. P. Orlando, S. Gustavsson, and W. D. Oliver, Applied physics reviews 6 (2019).
- [12] B. J. Chapman, E. I. Rosenthal, J. Kerckhoff, B. A. Moores, L. R. Vale, J. Mates, G. C. Hilton, K. Lalumiere, A. Blais, and K. Lehnert, Physical Review X 7, 041043 (2017).
- [13] Y.-Y. Wang, Y.-X. Wang, S. van Geldern, T. Connolly, A. A. Clerk, and C. Wang, Science Advances 10, eadj8796 (2024).
- [14] M. Gupta, G. V. Graziano, M. Pendharkar, J. T. Dong, C. P. Dempsey, C. Palmstrøm, and V. S. Pribiag, Nature communications 14, 3078 (2023).
- [15] M. Nadeem, M. S. Fuhrer, and X. Wang, Nature Reviews Physics 5, 558 (2023).
- [16] R. Upadhyay, D. S. Golubev, Y.-C. Chang, G. Thomas, A. Guthrie, J. T. Peltonen, and J. P. Pekola, Nature Communications 15, 630 (2024).
- [17] F. Ando, Y. Miyasaka, T. Li, J. Ishizuka, T. Arakawa, Y. Shiota, T. Moriyama, Y. Yanase, and T. Ono, Nature 584, 373 (2020).
- [18] A. Daido, Y. Ikeda, and Y. Yanase, Physical Review Letters 128, 037001 (2022).
- [19] C. Schmid, A. Jozani, R. Kleiner, D. Koelle, and E. Goldobin, arXiv preprint arXiv:2408.01521 (2024).
- [20] L. Labarca, O. Benhayoune-Khadraoui, A. Blais, and A. Parra-Rodriguez, Physical Review Applied 22, 034038 (2024).
- [21] N. Frattini, U. Vool, S. Shankar, A. Narla, K. Sliwa, and M. Devoret, Applied Physics Letters 110 (2017).
- [22] N. Frattini, V. Sivak, A. Lingenfelter, S. Shankar, and M. Devoret, Physical Review Applied 10, 054020 (2018).
- [23] Y.-M. Ren, X.-F. Pan, X.-Y. Yao, X.-W. Huo, J.-C. Zheng, X.-L. Hei, Y.-F. Qiao, and P.-B. Li, arXiv preprint arXiv:2411.06775 (2024).
- [24] A. Metelmann and A. A. Clerk, Physical Review X 5,

- 021025 (2015).
- [25] Y. Tanaka, B. Lu, and N. Nagaosa, Physical Review B 106, 214524 (2022).
- [26] S. Ghosh, V. Patil, A. Basu, Kuldeep, A. Dutta, D. A. Jangade, R. Kulkarni, A. Thamizhavel, J. F. Steiner, F. von Oppen, et al., Nature Materials 23, 612 (2024).
- [27] J. Ma, R. Zhan, and X. Lin, Advanced Physics Research , 2400180 (2025).
- [28] A. Sundaresh, J. I. Väyrynen, Y. Lyanda-Geller, and L. P. Rokhinson, Nature Communications 14, 1628 (2023).
- [29] M. Roig, P. Kotetes, and B. M. Andersen, Physical Review B 109, 144503 (2024).
- [30] Y. Mao, Q. Yan, Y.-C. Zhuang, and Q.-F. Sun, Physical Review Letters 132, 216001 (2024).
- [31] M. S. Anwar, T. Nakamura, R. Ishiguro, S. Arif, J. W. Robinson, S. Yonezawa, M. Sigrist, and Y. Maeno, Communications Physics 6, 290 (2023).
- [32] J. J. Cuozzo, W. Pan, J. Shabani, and E. Rossi, Physical Review Research 6, 023011 (2024).
- [33] Y.-Y. Lyu, J. Jiang, Y.-L. Wang, Z.-L. Xiao, S. Dong, Q.-H. Chen, M. V. Milošević, H. Wang, R. Divan, J. E. Pearson, et al., Nature communications 12, 2703 (2021).
- [34] A. Arora and P. Narang, arXiv preprint arXiv:2501.17924 (2025).
- [35] O. Matsyshyn and J. C. Song, arXiv preprint arXiv:2507.06290 (2025).
- [36] Y. Sung, L. Ding, J. Braumüller, A. Vepsäläinen, B. Kannan, M. Kjaergaard, A. Greene, G. O. Samach, C. McNally, D. Kim, et al., Physical Review X 11, 021058 (2021).
- [37] J. Ingla-Aynés, Y. Hou, S. Wang, E.-D. Chu, O. A. Mukhanov, P. Wei, and J. S. Moodera, Nature Electronics 8, 411 (2025).
- [38] H. Wu, Y. Wang, Y. Xu, P. K. Sivakumar, C. Pasco, U. Filippozzi, S. S. Parkin, Y.-J. Zeng, T. McQueen, and M. N. Ali, Nature 604, 653 (2022).
- [39] C. Ciaccia, R. Haller, A. C. Drachmann, T. Lindemann, M. J. Manfra, C. Schrade, and C. Schönenberger, Physical Review Research 5, 033131 (2023).
- [40] S. Bhowmik, D. Samanta, A. K. Nandy, A. Saha, and S. K. Ghosh, Communications Physics 8, 1 (2025).
- [41] C. Leroux, A. Parra-Rodriguez, R. Shillito, A. Di Paolo, W. D. Oliver, C. M. Marcus, M. Kjaergaard, A. Gyenis, and A. Blais, arXiv preprint arXiv:2209.06194 (2022).
- [42] J. Li, Z. Zhang, S. Wang, Y. He, H. Lyu, Q. Wang, B. Dong, D. Zhu, H. Matsuki, D. Zhu, et al., arXiv preprint arXiv:2506.17651 (2025).
- [43] Y. V. Fominov and D. Mikhailov, Physical Review B 106, 134514 (2022).
- [44] J.-X. Lin, P. Siriviboon, H. D. Scammell, S. Liu, D. Rhodes, K. Watanabe, T. Taniguchi, J. Hone, M. S. Scheurer, and J. Li, Nature Physics 18, 1221 (2022).
- [45] T. Kokkeler, A. Golubov, and F. Bergeret, Physical Review B 106, 214504 (2022).
- [46] R. S. Souto, M. Leijnse, and C. Schrade, Physical Review Letters 129, 267702 (2022).
- [47] B. Abdo, A. Kamal, and M. Devoret, Physical Review B—Condensed Matter and Materials Physics 87, 014508 (2013).
- [48] C. Schrade and V. Fatemi, Physical Review Applied 21, 064029 (2024).
- [49] V. Sivak, N. Frattini, V. Joshi, A. Lingenfelter, S. Shankar, and M. Devoret, Physical Review Applied

- **11**, 054060 (2019).
- [50] D. Kafri, C. Quintana, Y. Chen, A. Shabani, J. M. Martinis, and H. Neven, Physical Review A 95, 052333 (2017).
- [51] J. Koch, A. A. Houck, K. L. Hur, and S. Girvin, Physical Review A—Atomic, Molecular, and Optical Physics 82, 043811 (2010).
- [52] B. M. Anderson, R. Ma, C. Owens, D. I. Schuster, and J. Simon, Physical Review X 6, 041043 (2016).
- [53] F. Yan, P. Krantz, Y. Sung, M. Kjaergaard, D. L. Campbell, T. P. Orlando, S. Gustavsson, and W. D. Oliver, Physical Review Applied 10, 054062 (2018).
- [54] L. Ding, M. Hays, Y. Sung, B. Kannan, J. An, A. Di Paolo, A. H. Karamlou, T. M. Hazard, K. Azar, D. K. Kim, et al., Physical Review X 13, 031035 (2023).
- [55] S. A. Fldzhyan, M. Y. Saygin, and S. P. Kulik, Physical Review Research 3, 043031 (2021).
- [56] R. Stockill, M. Stanley, L. Huthmacher, E. Clarke, M. Hugues, A. Miller, C. Matthiesen, C. Le Gall, and M. Atatüre, Physical review letters 119, 010503 (2017).
- [57] W. K. Wootters, Physical Review Letters 80, 2245 (1998).
- [58] N. Nefedkin and A. Alù, IEEE Transactions on Microwave Theory and Techniques 72, 2130 (2024).
- [59] D. F. V. James, P. G. Kwiat, W. J. Munro, and A. G. White, Phys. Rev. A 64, 052312 (2001).
- [60] M. G. A. Paris and J. Řeháček, Quantum State Estimation, Lecture Notes in Physics, Vol. 649 (Springer, 2004).
- [61] A. I. Lvovsky and M. G. Raymer, Rev. Mod. Phys. 81, 299 (2009).
- [62] D. H. Mahler, L. A. Rozema, A. Darabi, C. Ferrie, R. BlumeKohout, and A. M. Steinberg, Phys. Rev. Lett. 111, 183601 (2013).
- [63] C. Ferrie, Phys. Rev. Lett. 113, 190404 (2014).
- [64] L. DiCarlo, J. M. Chow, J. M. Gambetta, L. S. Bishop, B. R. Johnson, D. I. Schuster, J. Majer, A. Blais, L. Frunzio, S. M. Girvin, and R. J. Schoelkopf, Nature 460, 240 (2009).
- [65] D. J. Egger and F. K. Wilhelm, Phys. Rev. Lett. 112, 240503 (2014).
- [66] R. C. Bialczak, M. Ansmann, M. Hofheinz, E. Lucero, R. McDermott, M. Neeley, A. D. OConnell, D. Sank, P. J. Steinmeyer, A. N. Cleland, and J. M. Martinis, Nat. Phys. 6, 409 (2010).
- [67] J. M. Gambetta, A. D. Córcoles, S. T. Merkel, J. M. Chow, J. A. Smolin, C. Rigetti, S. Poletto, B. L. T.

- Plourde, and M. Steffen, Phys. Rev. Lett. **106**, 030502 (2011).
- [68] C. Eichler, D. Bozyigit, C. Lang, L. Steffen, J. M. Fink, M. Baur, S. Filipp, M. P. da Silva, and A. Wallraff, Phys. Rev. Lett. 106, 220503 (2011).
- [69] M. Neeley, M. Ansmann, R. C. Bialczak, M. Hofheinz, N. Katz, E. Lucero, A. D. OConnell, D. Sank, J. Wenner, A. N. Cleland, and J. M. Martinis, Nature 467, 570 (2010).
- [70] A. Kamal, J. Clarke, and M. H. Devoret, Phys. Rev. B 84, 174510 (2011).
- [71] B. Abdo, K. M. Sliwa, L. Frunzio, and M. H. Devoret, Phys. Rev. X 3, 031001 (2013).
- [72] N. R. Bernier, L. E. Tóth, P. Koerber, J. K. Asboth, A. K. Feofanov, and T. J. Kippenberg, Nat. Commun. 8, 604 (2017).
- [73] L. Ranzani and J. Aumentado, New J. Phys. 17, 023024 (2015).
- [74] B. Kannan, M. J. Ruckriegel, D. L. Campbell, A. Frisk Kockum, J. Braumüller, D. K. Kim, M. Kjaergaard, P. Krantz, A. Melville, B. M. Niedzielski, et al., Nature 583, 775 (2020).
- [75] J. J. He, Y. Tanaka, and N. Nagaosa, Nature Communications 14, 3330 (2023).
- [76] T. Golod and V. M. Krasnov, Nature Communications 13, 3658 (2022).
- [77] S. Barzanjeh, M. Wulf, M. Peruzzo, M. Kalaee, P. Dieterle, O. Painter, and J. M. Fink, Nature communications 8, 953 (2017).
- [78] D. Zhang and J.-S. Tsai, Physical Review Applied 15, 064013 (2021).
- [79] J. Kerckhoff, K. Lalumière, B. J. Chapman, A. Blais, and K. Lehnert, Physical Review Applied 4, 034002 (2015).
- [80] N. Ofek, A. Petrenko, R. Heeres, P. Reinhold, Z. Leghtas, B. Vlastakis, Y. Liu, L. Frunzio, S. M. Girvin, L. Jiang, et al., Nature 536, 441 (2016).
- [81] V. Peano, C. Brendel, M. Schmidt, and F. Marquardt, Physical Review X 5, 031011 (2015).
- [82] P. Roushan, C. Neill, A. Megrant, Y. Chen, R. Babbush, R. Barends, B. Campbell, Z. Chen, B. Chiaro, A. Dunsworth, et al., Nature Physics 13, 146 (2017).
- [83] F. Arute, K. Arya, R. Babbush, D. Bacon, J. C. Bardin, R. Barends, R. Biswas, S. Boixo, F. G. Brandao, D. A. Buell, et al., Nature 574, 505 (2019).

Supplemetary Information for "Nonreciprocal quantum information processing with superconducting diodes in circuit quantum electrodynamics"

S1. Superconducting Diode Effect from an asymmetric SQUID Junction

Following [43, 46, 48], we assume a superconducting quantum interference device (SQUID) with asymmetric junction potentials that will lead to a Josephson Diode effect. The diode behavior stems from the simultaneous breaking of inversion symmetry breaking and time reversal symmetry breaking. In contrast to bulk superconductors, where the effect stems from Cooper pais formed across different Fermi surfaces, in JJ based methods the effect occurs through imperfect transmission or anomalous phase accumulation across the junction [15]. The nonreciprocal behavior of the diode will manifests itself in the resonator structure through the kinetic inductance of the resonator. The bias of the diode is fixed via \mathcal{T} -breaking agent through Φ_b and c_3 which stems from the third order expansion of the Josephson potential and the signal across the ports sets the notion of directionality through the diode.

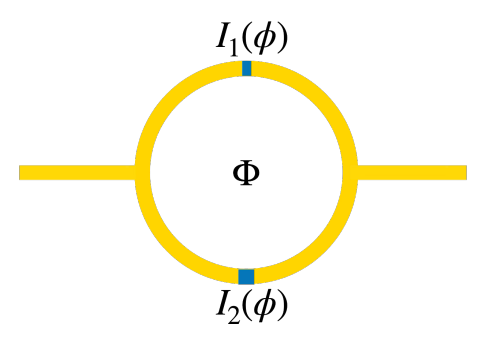


FIG. S1: Asymmetric SQUID with different CPRs $I_1(\phi)$ and $I_2(\phi)$ in the two JJs.

The the system Hamiltonian comprised of the diode coupler modeled as a capacitively shunted flux-tunable transmon comprised of two JJ's, transmission lines and interaction between them. Starting with the coupler systems we have the following Hamiltonian:

$$\frac{H_r}{\hbar} = 4E_c\hat{n} + U(\Phi) \tag{S1}$$

where $E_c = \frac{e^2}{2C}$ is the charge energy, \bar{n} the charge operator and $U(\Phi) = U_1(\Phi) + U_2(\Phi)$ represents the Josephson potential. The SQUID is pictured in Figure S1 showcasing a simple JD interferometer setup comprising of two JJs (blue) with a nonsinusoidal current-phase relationship (CPR). The SQUID is flux controlled via Φ . The diode effect stems from a simple model where two nonsinusoidal CPR's from the asymmetric junctions allow for higher order effects which are the crucial ingredient for nonreciprocity:

$$I_l(\Phi) = \frac{e\Delta^2 \tau_l}{2\hbar} \frac{\sin(\Phi)}{\epsilon_l(\Phi)} \tanh \frac{\epsilon_l(\Phi)}{2k_B T}$$
 (S2)

$$\epsilon_l(\Phi) = \Delta \sqrt{1 - \tau_l \sin^2 \frac{\Phi}{2}}.$$
 (S3)

The Josephson energy of each junction follows from CPR

$$U_l(\Phi) = -\Delta \sqrt{1 - \tau_l \sin^2 \frac{\Phi}{2}} \tag{S4}$$

In the SQUID with the two junction arrays the Josephson potential with an external flux Φ and a bias flux Φ_b can be readily defined as:

$$U(\Phi) = U_1(\Phi) + U_2(\Phi - \Phi_b) \tag{S5}$$

This model allows us to describe the SD effect.

S2. Transmission coefficient from classical input-output theory

We implement classical input-output theory on a two-port network such that input and output on two ports are described by $\{a_1, a_2\}$ and $\{b_1, b_2\}$. Assuming input at port 1 and output at port 2, the transmission coefficient is written as

$$S_{21} = \frac{b_2}{a_1} = \frac{Z_0}{Z_0 + Z(\omega)} \tag{S6}$$

where $Z(\omega) = R + i(\omega L - \frac{1}{\omega C})$. This leads us to define:

$$|S_{21}|^2 = \left| \frac{Z_0}{Z_0 + R + i(\omega L^{\pm} - \frac{1}{\omega C})} \right|^2$$
 (S7)

and after defining $\omega_0^{\pm} = \frac{1}{\sqrt{L^{\pm}C}}$ we obtain:

$$S_{21} = \frac{Z_0^2}{\frac{(Z_0 + R)^2}{4L^{\pm 2}} + (\omega - \omega_0^{\pm})^2} \frac{1}{4L^{\pm 2}}$$
 (S8)

where $A = \frac{Z_0^2}{4L^2}$ and $\kappa = \frac{(Z_0 + R)^2}{4L^2}$ such that:

$$S_{21} = \frac{A^{\pm}}{\kappa^{\pm} + (\omega - \omega_0^{\pm})^2}.$$
 (S9)

1. S3. Quantum analysis of diode nonreciprocity

Starting from Eq. (S1), we expand the Josephson potential into Fourier components around Φ_{\min}

$$U(\Phi) = \sum_{n} \frac{c_n}{n!} (\Phi - \Phi_{\min})^n, \tag{S10}$$

and denote the expansion coefficients $c_n = \partial_{\Phi}^n U(\Phi)$, and Φ_{\min} is self-consistently found by solving $c_1(\Phi) = 0$. We focus on the term $H_3 = (c_3/6)\Phi^3$, and write flux in terms of bosonic operators

$$\Phi(x) = \sum_{k} \Phi_{\text{zpf}} \left[\psi_k(x) a_k + \psi_k^*(x) a_k^{\dagger} \right]$$
 (S11)

where a_k is the bosonic operator, and $\psi_k(x) = u_k e^{ikx}$ is the mode function between the ports; $\Phi_{\rm zpf}$ is the flux at zero point fluctuation. We decompose flux into mean-field value and corresponding quantum fluctuations

$$\Phi = \Phi_b + \delta\Phi \tag{S12}$$

satisfying $\langle \Phi \rangle = \Phi_b$ and $\langle \delta \Phi \rangle = 0$. For bosonic operators this implies, $a_k = \alpha_k + d_k$ where $\langle a_k \rangle = \Phi_b \alpha_k$ is the mean-field expectation value satisfying $\langle \Phi \rangle = \Phi_b$ and $\langle d_k \rangle = 0$. With these definitions we can write

$$H_3 = \frac{c_3}{6} \prod_i \left(\sum_{k_i} \psi_{k_i} a_{k_i} \psi_{k_i}^* a_{k_i}^{\dagger} \right)$$
 (S13)

and represent flux as

$$\Phi = \mathcal{C} + X = \left(\sum_{k} \Phi_{\text{zpf}} \left[\psi_{k} \alpha_{k} + \psi_{k}^{*} \alpha_{k}^{*}\right]\right) + \left(\sum_{k} \Phi_{\text{zpf}} \left[\psi_{k} d_{k} + \psi_{k}^{*} d_{k}^{*}\right]\right)$$
(S14)

which together help us write

$$H_3 = \frac{c_3}{6} \left[\mathcal{C}^3 + 3\mathcal{C}^2 X + 3\mathcal{C}X^2 + X^3 \right]$$
 (S15)

where $C \neq 0$ captures $\Phi_b \neq 0$. Note that for $\Phi_b = 0$, the X^3 term given the three-wave mixing contribution, and for $\Phi_b \neq 0$ $3CX^2$ gives the leading order bilinear correction which can shift the frequency of Hamiltonian in Eq. (S1). Moving on, we assume $C \propto \Phi_b$ as a constant and express H_3 as

$$H_3 = \frac{Cc_3}{2} \Phi_{\text{zpf}}^3 \sum_{kk'} \psi_k \psi_{k'} d_k^{\dagger} d_{k'} = \sum_{kk'} \Lambda_{kk'} d_k^{\dagger} d_{k'}.$$
 (S16)

We now narrow our discussion to a two mode system such as $a \equiv a_k$ is the forward moving mode and $b \equiv a_{-k}$ is the backward moving mode. We can then write the Hamiltonian as

$$\tilde{H} = \begin{pmatrix} a^{\dagger} & b^{\dagger} \end{pmatrix} \begin{pmatrix} \omega_k + \Lambda_{k,k} & \Lambda_{k,-k} \\ \Lambda_{-k,k} & \omega_{-k} + \Lambda_{-k,-k} \end{pmatrix} \begin{pmatrix} a \\ b \end{pmatrix}, \tag{S17}$$

and it can be seen that both frequency shift and mode mixing arise from the interplay of $\Phi_b, c_3 \neq 0$. However, mode mixing effects scale as Λ^2 and are thus even with Φ_b . On the contrary, frequency shift is leading order in Λ and thus emerge as tunable nonreciprocal signature. The corresponding difference in frequency of forward and backward mode then reads

$$\delta\omega_r = \omega_k - \omega_{-k} = \frac{Cc_3}{2} \Phi_{\text{zpf}}^3 \left[|u_k|^2 - |u_{-k}|^2 \right].$$
 (S18)

Noting that $\mathcal{C} \propto \Phi_b$, $c_3(\Phi_b) = -c_3(-\Phi_b)$ and $[|u_k|^2 - |u_{-k}|^2]$ flips sign with Φ_b , we deduce that $\omega_k - \omega_{-k}$ is odd in Φ_b , and reproduce Eq. (5) of the main text.

S4. Diode Spectroscopy

Here we detail the spectroscopy calculations using equations of motion and quantum Hamiltonian. Combining the system Hamiltonian and analyzing the system with the transmission line, where the two ends of the transmission lines are coupled with rate κ_1 and κ_2 , we can proceed and define the equations of motion coming from the Heisenberg-Langevin equations:

$$\dot{a} = -\frac{i}{\hbar} [H_r, a] - \frac{\kappa}{2} a + \sqrt{\kappa_1} a_{in} + \sqrt{\kappa_2} b_{in}$$

$$a_{out} = a_{in} - \sqrt{\kappa_1} a$$

$$b_{out} = b_{in} - \sqrt{\kappa_2} a$$
(S19)

where $\kappa = \kappa_1 + \kappa_2$ represents the total decay. $a_{in}(a_{out})$ represents the input (output) ports of the system. The system is driven and probed with the standard Hamiltonian framework via $H_D = (\epsilon_p e^{-i\omega_p t} a^{\dagger} - h.c) + (\epsilon_{pr} e^{-i\omega_{pr} t} a^{\dagger} - h.c.)$ with drives $\epsilon_p = i\sqrt{\kappa}\epsilon_p$ and $\epsilon_{pr} = i\sqrt{\kappa}\epsilon_{pr}$ as well as frequencies ω_p and ω_{pr} . We work in the rotating frame at the pump rate and also linearize around small quantum fluctuations such that $a(t) = \alpha e^{-i\omega_p t} + \delta a(t)$, where α is the classical amplitude coming from the coherent pump and δa the fluctuations. One can then divide the equations of motion in two parts: one for the steady state amplitude of the classical coherent field and one for the fluctuations:

$$\dot{\alpha} = -i(\Delta + \delta\omega_r + \frac{\Lambda}{2}|\alpha|^2 - i\frac{\kappa}{2})\alpha + \epsilon_p$$

$$\dot{\delta a}(t) = -i(\Delta_{eff} - i\frac{\kappa}{2})\delta a - i\lambda\delta a^{\dagger} + \epsilon_{pr}e^{-i\Omega t}$$
(S20)

where $\Delta_{eff} = \Delta + \delta\omega_r$, $\Delta = \omega_0 - \omega_p$ and $\lambda = \Lambda |\alpha|^2$. With $\Lambda \neq 0$ we have included the Kerr nonlinearity for completeness. We apply the Fourier transform $\delta a(t) = \int d\Omega e^{-i\Omega t} d[\Omega]$ with $\Omega = \omega_{pr} - \omega_p$ the shifted probe frequency

$$\begin{pmatrix} i\Omega + \frac{\kappa}{2} + i\Delta_{eff} & i\lambda \\ -i\lambda^* & i\Omega + \frac{\kappa}{2} - i\Delta_{eff} \end{pmatrix} \begin{pmatrix} \delta a[\Omega] \\ \delta a^{\dagger}[-\Omega] \end{pmatrix} = \begin{pmatrix} \sqrt{\kappa_1} a_{in}[\Omega] + \sqrt{\kappa_2} b_{in}[\Omega] \\ \sqrt{\kappa_1} a_{in}^{\dagger}[-\Omega] + \sqrt{\kappa_2} b_{in}^{\dagger}[-\Omega] \end{pmatrix}$$
(S21)

where we define $M[\Omega]$ as the system matrix, where the boundary conditions remain unchanged with the linearized term $a = \alpha + \delta a$. We now invert $M[\Omega]$ to obtain the scattering parameters:

$$\chi(\Omega) = (i\Omega I - M[\Omega])^{-1} = \frac{1}{D(\Omega)} \begin{pmatrix} i\Omega + \frac{\kappa}{2} - i\Delta_{eff} & -i\lambda^* \\ i\lambda & i\Omega + \frac{\kappa}{2} + i\Delta_{eff} \end{pmatrix},$$

$$D(\Omega) = (i\Omega + \frac{\kappa}{2})^2 + \Delta_{eff}^2 - |\lambda|^2.$$
(S22)

Now using the input-output relations and injecting an idler signal at $\omega = \Omega + \omega_p$ through port 1 such that $a_{in}[\Omega] = A_{in}$ and $b_{in}[\Omega] = 0$ we obtain the forward transmission spectrum. The fluctuation at ω becomes:

$$\delta a[\Omega] = \chi_{11}(\Omega)\sqrt{\kappa_1}A_{in}[\Omega] + \chi_{12}(\Omega)\sqrt{\kappa_1}A_{in}[-\Omega]$$
(S23)

where $\chi(\Omega)_{ii} = (i\Omega I - M)_{ii}^{-1}(\Omega)$ is the susceptibility element from the linear response. The forward transmission coefficient then becomes:

$$S_{21}(\Omega) = \frac{b_{out}[\Omega]}{a_{in}[\Omega]} = -\sqrt{\kappa_1 \kappa_2} \chi_{11}(\Omega) - \sqrt{\kappa_1 \kappa_2} \chi_{12}(\Omega) \frac{A_{in}[-\Omega]}{A_{in}[\Omega]}$$
 (S24)

where for backward transmission, we repeat the same method but instead inject the probe tone through b_{in} .